First gas and thermal measurements at the summit of Gamalama reveal a dominated hydrothermal system behind the numerous eruptive events

Syegi KUNRAT[1], Philipson BANI[2], Nia HAERANI[1], Ugan SAING[1], Alessandro AIUPPA[3], Devy Kamil SYAHBANA[1]

[1]Center for Volcanology and Geological Hazard Mitigation, Indonesia,
[2]The French Research Institute for Development, France,
[3]Università di Palermo, Italy

Abstract

The first gas and thermal measurements at the summit of the Gamalama volcano indicate that the system is dominated by hydrothermal processes. This is highlighted by the prevalence of H_2S over SO_2 (H_2S/SO_2 = 2-8), a high CO_2/SO_2 ratio (76-201), and a low heat transfer (3.0 MW) to the surface. A relative variation in gas composition is observed along the degassing fracture zone, possibly due to inconsistent S scrubbing. Despite this surface hydrothermal signature, the system displays a high gas equilibrium temperature (425-480°C) which emphasizes that the ascent fluid is not exclusively derived from a boiling hydrothermal aquifer, instead, the cooling and crystallizing basaltic magmatic source continue to inject magmatic fluids into the system. This dominated hydrothermal activity on Gamalama possibly persisted over the last two decades, during which a high number of eruptive events were witnessed. The period coincides as well with the occurrence of large fractures at the summit that shifted the volcanic activity from the center of the crater to the peripheral fractures zone. These fractures have likely weakened the hydrothermal seal, allowing the pressure developed by the hydrothermal system, promoted by the high annual rainfall, to rapidly exceeds the tensile strength of the seal leading to numerous phreatic eruptions.

1/ Introduction

Gamalama is a stratovolcano with a near-perfect cone-shape with an aerial diameter of 12 km. Located off the coast of Halmahera island, this 1715 m high volcano is one of the 5 active volcanoes of Halmahera arc (Fig.1). Since 1510, Gamalama has experienced 66 confirmed eruptions highlighted by a dense column of ash, ejected incandescent material, voluminous lava flow, pyroclastic flow as well as lahar (GVP, 2013). The volcano host a city of about 200,000 inhabitant on its southeastern flank (Fig.1) – a perfect illustration of a City on Volcano. In 1988, 3500 inhabitants were evacuated out of the island in response to a strong eruptive event. In 1983 and 2011, thousands of inhabitants were displaced from an exposed zone to safer areas (GVP, 2013). Due to abundant ash emissions, the Sultan Babullah International airport was regularly forced to closed. This was the case on July 18, 2005, on Aug. 3-4, 2017, and Oct. 4, 2018 (GVP, 2013). About 11% of the eruptive events are classified as moderate-to-large eruptions with VEI 3, whilst 70% are considered as moderate eruptions with VEI 2 (GVP, 2013). The major eruptive event on Gamalama

occurred in September 1775, forming the maar of Tolire and buried the village of Soela Takomi, killing 141 inhabitants (Dasar, 2011, Mei et al., 2016). More recently, in 2011, a lahar event claimed 4 deaths (GVP, 2013), thus a total of 145 direct victims are recorded from Gamalama volcanic activities over the last two and a half centuries.

The particularity on Gamalama volcano, according to the Center of Volcanology and Geological Hazard Mitigation (CVGHM), the institution in charge of the volcano monitoring in Indonesia, is its capacity to develop eruptive events with very short precursory signals or only a few volcanic quakes before eruptions (volcano news: www.vsi.esdm.id). Such a character constitutes a huge challenge for Gamalama volcano observatory who struggle to provide timely warnings to inhabitants. To gain insights into the recent volcanic activity of Gamalama, a fieldwork was carried out at the summit on September 21, 2018, during which the heat distribution, the radiant flux, and the chemical composition of the gas plume were characterized for the first time. Here we present the results of this field investigation.

2/ Methodology

The gas composition on Gamalama was measured using a Multi-component Gas Analyser System (Multi-GAS; Aiuppa et al., 2005; Shinohara, 2005). This portable instrument measures the concentrations of CO_2, SO_2, H_2S, H_2, as well as pressure, temperature, and relative humidity. This latter was converted to H_2O using the formula outlined in Buck (1981):

$H_2O = 6.1121*(1.0007+3.46P^{-6})*\exp((17.502*T)/249.97+T)*RH*104*P^{-1}$.

The CO_2 gas is detected by near dispersive infrared spectroscopy (range 0-60,000 ppm) while SO_2, H_2S, H_2 gases were quantified using specific electrochemical sensors models (range 0-200 ppm). Data were processed and analyzed using ratiocalc software (Tamburello, 2015). During field measurements, the multiGAS was positioned at 3 different degassing points at the summit.

To characterize the heat distribution and heat flux on the summit of Gamalama, a PI640 OPTRIS was deployed on the crater rim. This miniature infrared camera weighs 320g, including a lens of 62°x49° FOV, f=8 mm, and a dynamic range equivalent to the radiant temperature of -20°C to 900 °C. The detector has 640x480 pixels and the operating waveband is 7.5-13 µm. The maximum frame rate is 80 Hz. The radiant flux (Q_{rad}) estimation is obtained using the following equation: $Q_{rad} = A\varepsilon\sigma(T_s^4 - T_a^4)$, where A is the hot surface, ε is the emissivity (0.9 for basalt), σ is the Stefan-Boltzmann constant ($5.67x10^{-8}$ W m^{-2} K^{-4}), T_s is the hot surface temperature and T_a is the ambient temperature. Thermal results are corrected for oblique viewing angle, following the approach detailed in Harris (2013) and the temperature values are corrected for atmospheric influence relying on ACPC models (https://atmcorr.gsfc.nasa.gov/) and validated with closer thermal recording. The radiant flux was calculated at 5 different temperature ranges (32-35°C; 36-40°C, 41-45°C, 46-50°C and >57°C) then summed for the entire zone of interest (Table 1). The value below 32°C was difficult to discriminate from the background and therefore considered as background.

3/ Result

The thermal infrared camera survey on Gamalama indicates that the heated surface is relatively confined to the western part of the crater which prolonged outside the crater along the southwest fracture zone (Fig.2). The maximum temperature of ~125°C was recorded at that southwest fracture zone. The heated surface in the main crater is equivalent to ~4500 m^2 whilst along the southwest fracture zone, ~310 m^2 of the surface is heated beyond the background level (Table 1). The total radiant flux calculated for these heated surfaces is 3.0 MW, including 2.7 MW of heat through the crater and 0.3 MW through the southwestern fracture zone. However, this latter value should be considered minimum since the area is the main degassing zone, thus gas may prevent the thermal radiation, as seen on Etna by Sawyer and Burton (2006). The gas released from the crater is negligible in comparison to the southwestern fracture zone.

The multigas measurement results obtained on Gamalama highlight different gas compositions from the three recording points (Fig.3, Table 2). At MG1, the highest recording position (1698 m), results indicate a strongly diluted gas with H_2O, CO_2, SO_2, H_2S and H_2 concentrations of 7000-14000, 450-770, 0.05-0.13, 0.3-0.4 and 2.0-4.0 ppm v respectively. There is no correlation between these gas components, thus no acceptable gas ratio can be obtained at MG1. However, this near absence of SO_2 and H_2S (Fig.3), contrasts with the abundance of CO_2 and H_2, reflecting a diffusion to the surface (Rye 2005, Ohmoto and Rye 1979; Rye 1993; Giggenbach 1997), where less reactive gas such as CO_2 and H_2 persist at the surface. At the recording point MG2, situated ~20 m below MG1, the H_2O, CO_2, SO_2, H_2S, and H_2 concentrations correspond to 3000-12000, 395-550, 0.2-1.2, 0.4-6.5 and 0.6-4.0 ppm v respectively. There is a decrease in concentration for H_2O, CO_2, and H_2 between MG1 and MG2, whilst SO_2 and H_2S show an increase in concentration. The gas is less diluted compare to MG1, thus good correlations are obtained between gas components, with H_2O/SO_2, CO_2/SO_2, H_2S/SO_2 and H_2/SO_2 ratios of 5895±2979, 201±50, 7.9±0.9, and 1.4±0.9 respectively. At the measurement point MG3, located more than 50 m below MG1, the gas has the lowest concentration of H_2O (1000-7000 ppm v) and the highest SO_2 content (0.3-1.6 ppm v). The CO_2 (360-490 ppm v), H_2S (0.1-0.9 ppm v), and H_2 (0.0-3.5 ppm v) show relative decrease concentrations in comparison to MG2. The gas to SO_2 ratios at MG3 (Fig.4) correspond to 3169±1144, 76±12, 2.5±0.3 and, 1.2±1.0 for H_2O/SO_2, CO_2/SO_2, H_2S/SO_2, and H_2/SO_2 respectively. Assuming that this less diluted gas at MG3 can be representative of the system, given the highest SO_2 concentration, then Gamalama volcano releases a H_2O-rich gas, representing nearly 97.5% of the plume content. The other gas components represent 2.3%, 0.03%, 0.08% and 0.04% for CO_2, SO_2, H_2S and H_2 respectively.

4/ Discussion

4-1/ Domninated hydrothermal manifestation

Gas measurement results indicate a prevalence of H_2S over SO_2 with the H_2S/SO_2 ratio of 2-8 (Table 2, Fig.4) suggesting an effective conversion from SO_2 to H_2S according to the following reaction(Holland, 1965): $SO_2+4H_2O \rightarrow H_2S + 3H_2SO_4$. However, when the fluid ascent, it also interacts with the rock surface,

and subsequently the SO_2 is reduced by the FeO of the rock phase, according to Giggenbach (1987): $SO_2+6(FeO)+H_2O \rightarrow H_2S+6(FeO_{1.5})$. The efficiency of the rock buffer in converting the SO_2 to H_2S is likely to be a function of the intensity and duration of fluid-rock contact (Giggenbach, 1987). As such, the high H_2S/SO_2 ratio on Gamalama suggests prolonged fluid-rock interaction, which contrasts with other systems like Bromo (Aiuppa et al., 2014), Dukono (Bani et al., 2018) or Gamkonora (Saing et al.,2020) where faster rising magmatic fluids through well-defined channels enhance low H_2S/SO_2 ratios. The high CO_2/SO_2 ratio of 76-201 obtained on Gamalama is well above the magma value of 6-9 or 4 obtained on Merapi (Fisher, 2008) and Bromo (Aiuppa et al., 2014) respectively. However, such high CO_2/SO_2 values are common in hydrothermal systems given the less sensitive to the scrubbing of CO_2 due to its lower aqueous solubility and reactivity (Symonds et al., 2001). Gamalama degassing during this work is thus dominated by hydrothermal processes. This is supported by the gas composition of MG2 and MG3 within the CO_2-H_2O-S_T diagram (Fig.5). The gases plot along the H_2O-CO_2 axis, within the area of hydrothermal gas composition (Fisher and Chiodini, 2015), comparable to the Papandayan hydrothermal system. Gas from other volcanoes, including Bromo (Aiuppa et al., 2015), Sirung (Bani et al., 2017), Dukono (Bani et al., 2018) and Gamkonora (Saing et al., 2020) are plotted in the magmatic area. Gas composition at MG3, situated about 35 m below MG2, displays relatively lower ratios of H_2O/SO_2, CO_2/SO_2, H_2S, and H_2/SO_2 (Table 2, Fig.4). This relative distinct gas composition between MG2 and MG3 is possibly due to slower fluid ascent to the surface, allowing S scrubbing (Symonds et al., 2001) to be more effective at MG2. In contrast, the puffing dynamic at MG3, compare to continuous degassing at MG2 (Fig.3), indicates that the system develops pressure, possibly at a deeper location that enables relatively faster gas ascent to the surface at MG3. Note that this MG3 point is situated towards the end of the southwestern fracture, where the gas flow path to the surface is likely less defined (Fig.3).

This hydrothermal character of Gamalama is coherent with the low heat flux of 3 MW obtained in this work (Table 1) and 5 MW highlighted by MODVOLC on Aug. 4; 2003 outside eruptive period, (http://modis.higp.hawaii.edu/). For comparison, these values are far lower than the Vulcano hydrothermal system, where Harris and Maciejewski (2000) obtained 45-67 MW of heat flux. However, during Sep. 2012 eruption of Gamalama (GVP, 2013) MODVOLC established a heat flux of 44 MW, which thus indicates that thermal energy at the surface of Gamalama is subjected to change with the activity. In that respect, regular thermal and gas measurements can contribute to the monitoring network on Gamalama, since the evolution of fluid circulations is likely to enhance changes in gas composition and facilitate heat transfer to the surface.

4-2/ Magmatic contribution

Despite the hydrothermal manifestation evidenced in this work, characterized by the gas composition and the low heat flux, Gamalama has experienced strong magmatic activities in the past with incandescent projections in 1980, 1983, 1990 and 1993 (GVP, 2013), whilst lava flow occurred in 1983 and 2015 (GVP, 2015). DOAS gas measurements carried during the July 2015 eruption indicate a strong magmatic degassing

with a mean SO_2 flux of 1235 t d^{-1} (Table 3). This figure is much higher than the magmatic degassing at Dukono (820 t SO_2 d^{-1}; Bani et al., 2018). It is thus likely that the 2018 manifestation on Gamalama, as observed in this work, was possibly sustained by a progressively cooling magma.

The gas equilibrium temperature, obtained by resolving together the SO_2/H_2S vs. H_2/H_2O redox equilibria (Aiuppa et al., 2011; Moussallam et al., 2017) corresponds to 425-480°C, much higher than the maximum temperature observed with the infrared camera (Fig.2, Table 1). Such a high value suggests that the equilibrium temperature was reached below the surface and the hot fluid may transfer parts of its heat to the surrounding rocks during its final ascent. Assuming that the above equilibrium gas temperature is representative of the system, then the gas released at Gamalama is not exclusively derived from a boiling hydrothermal aquifer, where the temperature is generally below 250°C (Giggenbach, 1980; Chiodini and Marini, 1998). Instead it likely derives from the combined contributions from both, the magma and the hydrothermal processes. If plotting these gas temperatures against the CO_2/S_T ratios of 22-23, where S_T corresponds to the combined molar values of SO_2 and H_2S, Gamalama gas appears in the mixed zone (Fig.6; Aiuppa et al, 2017), confirming a contribution from the magma, similar to Papanayan (*Fisher and Chiodani, 2015*).

Bulk rock composition of the fresh rock sampled in 2018 (this work) and analyzed using ICP AES at the LMV (Laboratoire Magmas et Volcan) indicates the Gamalama is sustained by a basaltic magma (Fig.7). The 1907 lava flow and the ejected material of the 1990 eruption are also issued from a basaltic magma (Mawardi et al., 1991). Note that this basaltic composition contrasts with the more evolved melt sources on other volcanoes of the same Halmahera arc, including Gamkonora, Dukono, and Ibu. Such change suggests a complex geodynamic setting in the region (Fig.7) which is yet to be constrained.

4-2/ Fractures and phreatic events

On October 4, 2018, 23 days following our fieldwork at the summit, Gamalama went through an eruptive event with no precursory signals (GVP, 2018). Such a sudden and short eruptive event is typical of a phreatic eruption (Stix and de Moor, 2018). The event lasted 3 days and has released 30 t d^{-1} of SO_2 (GVP, 2018), much lower than the 1235 t d^{-1} of the 2015 eruption (Table 3), in accord with the phreatic nature of the event. Since 1510, Gamalama has experienced two episodes of an increasing number of eruptive events (Fig.8). The first increase was in the mid-19th-Century but it is unclear if the increase reflects the real behavior of the volcano. The period however coincides with the occurrence of the Dutch colony, during which more reports about volcanic eruptive activities became available (Dasar, 2011). The second increasing number of eruptive events that commenced in 2003 has 9 (7 confirmed) eruptions. Six out of the 9 eruptions (in 2007, 2008, 2012, 2014, 2016, 2018) displayed a phreatic signature with low intensity (VEI 1) and short duration (1-7 days) (GVP, 2013), whilst 3 other eruptions (in 2003, 2011 and 2015), of relatively higher intensity (VEI 2) and lasted between 18 and >60 days (GVP, 2013) suggesting a magmatic contribution. There was no significant evolution of the melt source on Gamalama between 1907, 1990, and 2018, as highlighted by the rock chemistry (Fig.7), which suggests no significant change of magma supply. Instead the cooling and

crystallizing of the Gamalama magma source may release and supply the required magmatic gas behind the volcanic activity, similar to Aso and Ontake volcanoes (Stix and de Moor, 2018). When magmatic fluid is injected into the hydrothermal system, it condenses and vaporizes the liquid hydrothermal water. Such a process that occurs at high temperatures may induce host rock alteration and sulfur precipitates (Christenson et al., 2010), leading ultimately to the development of a hydrothermal seal (Fig. 9, Stix and de Moor, 2018). This latter plays a direct role in the explosivity of phreatic eruption. When the seal is in place, overpressure can be achieved with the ascending hydromagmatic fluids and subsequently erupt as a phreatic or phreatomagmatic event. On Gamalama, this hydrothermal seal is possibly disrupted by the large fractures, formed at the summit between 2002 and 2011, according to the series of cloud-free satellite pictures available from google earth (Fig.8). Indeed, the summit morphology of Gamalama has evolved from a well circular central crater in 2002 to a fractured crater in the present time. The main active zone has subsequently shifted from the central to the peripheral fracture zones over the same period (Fig.8). This morphology evolution coincides with the increase of eruptive events, supporting the hypothesis of hydrothermal seal disruption. Hence the pressure developed by Gamalama hydrothermal system, promoted by the high annual rainfall (>2000 mm) may rapidly exceed the tensile strength of the disrupted seal, leading to the increased number of phreatic events (Houghton et al., 2015). Periodically, the Gamalama melt source releases magmatic fluid, when the overpressure exceeds the tensile strength of the enclosed carapace at deep (Stix and de Moor, 2018), leading to intermittent magmatic eruptions.

It is unclear how the fractures are formed, however, these are common by-products of volcanic activity (Lanzafame et al., 2003). They are generally made up of extensional fractures and normal faults, associated with dike emplacements (Rubin and Pollard, 1998; Opheim and Gudmundsson, 1989; Mastin and Pollard, 1988; Peacock and Parfitt, 2002; Lanzafame et al., 2003). The 2003 eruptive event on Gamalama which lasted more than 2 months with a series of strong explosions, ashy columns up to 2 km, and a reported pyroclastic flow may be associated with the fracture formation. Alternatively, the active tectonic region of North Maluku with more than 150 seismic events (M≥4) per year within the 200 km radius around Gamalama (https://earthquake.usgs.gov/) may contribute to the formation of Gamalama summit fractures. But that is beyond the scope of this work.

5/ Conclusion

The gas composition obtained at the summit of the Gamalama volcano indicates a dominated hydrothermal system, highlighted by the prevalence of H_2S over SO_2 (H_2S/SO_2 = 2-8) and a high CO_2/SO_2 ratio of 76-201. A relative variation in gas composition at different measurement points is observed, due to inconsistent S scrubbing along the degassing fracture zone. The heat transferred to the surface by the system corresponds to only 3.0 MW, in accord with the dominant of hydrothermal processes. However, the high gas equilibrium temperature of 425-480°C indicates that the ascent fluid is not exclusively derived from a boiling hydrothermal aquifer, instead, the cooling and crystallizing basaltic melt source continues to supply magmatic fluids into the system. This hydrothermal activity on Gamalama has persisted nearly two decades, a period

during which an elevated number of eruptions were witnessed on the volcano. It is thus likely that summit large fractures, developed since 2002 have weakened the hydrothermal seal, allowing the pressure developed by the hydrothermal system, promoted by the high annual rainfall, to rapidly exceeds the tensile strength of the seal leading to numerous phreatic eruptions.

Acknowledgements

We acknowledge the field support from the Gamalama observatory. The research leading to these results has received support from JEAI-COMMISSION under the collaboration between CVGHM and IRD.

References

Aiuppa, A., Federico, C., Giudice, G., Gurrieri, S., 2005. Chemical mapping of a fumarolic field: La Fossa Crater, Vulcano Island (Aeolian Islands, Italy). Geophys. Res. Lett. 32(13), L13309. http://dx.doi.org/10.1029/2005GL023207.

Aiuppa, A., Bani, P., Moussallam, Y., DiNapoli, R., Allard, P., Gunawan, H., Hendrasto ,M., Tamburello ,G., 2015. First determination of magma-derived gas emissions from Bromo volcano, eastern Java (Indonesia). J Volcanol Geotherm Res, 304, p.206-213, DOI:10.1016/j.jvolgeores.2015.09.008.

Aiuppa, A., Fischer, T.P., Plank, T., Robidoux, P., Di Napoli, R., 2017. Along-arc, inter-arc and arc-to-arc variations in volcanic gas CO_2/S_T ratios reveal dual source of carbon in arc volcanism. Earth-Science Reviews, 168, 24-47.

Bani, P., Alfianti, H., Aiuppa, A., Oppenheimer, C., Sitinjak, P., Tsanev, V., Saing, U.B., 2017. First study of the heat and gas budget for Sirung volcano, Indonesia. Bull. Volcanol., 79:60. https://doi.org/10.1007/s00445-017-1142-8.

Bani P., Tamburello G., Rose-Koga E., Liuzzo M., Aiuppa A. Cluzel N., Amat I., Syahbana D.K., Gunawan H., Bitetto M., 2018. Dukono, the predominant source of volcanic degassing in Indonesia, sustained by a depleted Indian-MORB. Bulletin of Volcanology vol.80, 5, DOI:10.1007/s00445-017-1178-9.

Buck, A.L., 1981. New equations for computing vapor pressure and enhancement factor. J Appl Meteorol 20:1527–1532.

Christenson, B.W., Reyes, A.G., Young, R., Moebis, A., Sherburn, S., Cole-Baker, J., Britten, K., 2010. Cyclic processes and factors leading to phreatic eruption events: insights from the 25 September 2007 eruption through Ruapehu crater lake, New Zealand. J Volcanol Geotherm Res 191:15–32. https://doi.org/10.1016/j.jvolg eores .2010.01.008.

Data Dasar Gunung Api, Wilaya Timur, 2011. edisi kedua. Kementerian Energi dan Sumber Daya Mineral, Badan Geologi, pp. 1-450.

Fischer, T.P., 2008. Fluxes of volatiles (H_2O, CO_2, N_2, Cl, F) from arc volcanoes. Geochem. J. 42:21-38.

Fischer, T.P., Chiodini, G., 2015. Volcanic, Magmatic and Hydrothermal Gases. In Encyclopaedia of Volcanoes, 2nd Edition, 779–797 https://doi.org/10.1016/B978-0-12-385938-9.00045-6.

Giggenbach, W.F., 1987. Redox processes governing the chemistry of fumarolic gas discharges from White Island, New Zealand. Appl. Geochem., 2, 143-161.

Giggenbach, W.F., 1997. The origin and evolution of fluids in magmatichydrothermal systems. In: Barnes HL (ed) Geochemistry of hydrothermal ore deposits, 3rd edn. Wiley, New York, pp 737–796.

Global Volcanism Program, 2013. Gamalama (268060) in Volcanoes of the World, v. 4.8.5. Venzke, E (ed.). Smithsonian Institution. https://doi.org/10.5479/si.GVP.VOTW4-2013.

Global Volcanism Program, 2015. Report on Gamalama (Indonesia) (Venzke, E., ed.). Bulletin of the Global Volcabism Network, 40:12. Smithsonian Institution. https://doi.org/10.5479/si.GVP.BGVN201512-268060.

Global Volcanism Program, 2018. Report on Gamalama (Indonesia) (Venzke, E., ed.). Bulletin of the Global Volcanism Network, 43:11. Smithsonian Institution. https://doi.org/10.5479/si.GVP.BGVN201811-268060.

Harris, A.J.L., Maciejewski, A.J.H., 2000. Thermal surveys of the Vulcano Fossa fumaroles field 1994-1999: evidence for fumarole mitigation and sealing. J. Volcanol. Geothermal Res., 102, 119-147.

Harris, A., 2013. Thermal Remote Sensing of Active Volcanoes, A user's Manual. Cambridge University Press, UK, pp. 1-728.

Holland, H.D., 1965. Some applications of thermochemical data to problems of ore deposits II. Mineral assemblages and the composition of ore-forming fluids. Econ. Geol. 60, 1101-1166.

Houghton, B., White, J.D.L., Van Eaton, A.R., 2015. Phreatomagmatic and Related Eruption Styles. The Encyclopedia of Volcanoes, 537-552. http://dx.doi.org/10.1016/B978-0-12-385938-9.00030-4.

Lanzafame, G., Neri, M., Acocella, V., Billi, A., Funiciello, R., Giordano, G., 2003. Structural features of the July-August 2001 Mount Etna eruption: evidence for a complex magma supply system. J. Geological Society, London, 160, 531-544.

Mastin, L.G. & Pollard, D.D. 1988. Surface deformation and shallow dyke intrusion processes at Inyo craters, Long Valley, California. Journal of Geophysical Research, 93, 13221–13235.

Mawardi, R., Zaennudin, A., Kusdinar, E., Yohana, T., 1991. Penyelidikan Petrokimia dan potensial diri G. Gamalama, Ternate, Maluku, Directororat Vukanologi.

Mei, E.T.W., Sari, T.M., Fajarwati, A., Safitri, D., 2016. Assessing the Social Economic and Physical Vulnerabilities to Gamalama Volcanoes. Advances in Social Science, Education and Humanities Research, volume 79.

Ohmoto, H., Rye, R.O., 1979. Isotopes of sulfur and carbon. In: Barnes HL (ed) Geochemistry of hydrothermal ore deposits, 2nd edn. Wiley, New York, pp 509–567.

Opheim, J.A. & Gudmundsson, A. 1989. Formation and geometry of fractures and related volcanism of the Krafla fissure swarm, northeast Iceland. Geological Society of America Bulletin, 101, 1608–1622.

Peacock, D.C.P. & Parfitt, E.A. 2002. Active relay ramps and normal fault propagation on Kilauea Volcan Hawaii. Journal of Structural Geology, 24, 729–742.

Rubin, A.M. & Pollard, D.D. 1988. Dyke-induced faulting in rift zones of Iceland and Afar. Geology, 16, 413–417.

Rye, R.O., 2005. A review of the stable-isotope geochemistry of sulfate minerals in selected igneous environments and related hydrothermal systems. Chem Geol 215:5–36.

Rye, R.O., 1993. The evolution of magmatic fluids in the epithermal environment: the stable isotope perspective. Econ Geol 88:733–753.

Saing, U.B, Bani, P., Haerani, N., Aiuppa, A., Primulyana, S., Alfianti, H., Syahbana, D.K., Kristianto, 2020. First characterization of Gamkonora gas emission, North Maluku, East Indonesia. Bull. Volcano, https://doi.org/10.1007/s00445-020-01375-7.

Sawyer, G.M., Burton, M.R., 2006. Effects of a volcanic plume on thermal imaging data. Geophys. Res. Lett., 33, L14311, doi:10.1029/2005GL025320.

Shinohara, H., 2005. A new technique to estimate volcanic gas composition: plume measurements with a portable multi-sensor system. J. Volcanol. Geotherm. Res. 143, 319–333.

Symonds, R.B., Gerlach, T.M., Reed, M.H., 2001. Magmatic gas scrubbing: implications for volcano. monitoring. J. Volcanol. Geotherm. Res. 108, 303–341.

Stix, J. and de Moor, M., 2018. Understanding and forecasting phreatic eruptions driven by magmatic degassing. Earth, Planets and Space (2018) 70:83 https://doi.org/10.1186/s40623-018-0855-z.

Tamburello, G., 2015. Ratiocalc: software for processing data from multicomponent volcanic gas analyzers. Comput Geosci 82:63–67. https://doi.org/10.1016/j.cageo.2015.05.004.

Tables and captions

Table 1. Radiant flux from Gamalama volcano.

Main Crater				**Southern fracture zone**			
Zone of interest (m^2)		19674				2186	
Temp. range	**Corrected mean temp. (°)**	**Surface per Temp. range (%)**	**Mean Radiant flux (MW)**	**Temp. range**	**Corrected mean temp. (°)**	**Surface/Temp. range (%)**	**Mean Radiant flux (MW)**
32-35 °C*	102.9	17.5	**2.0**	35-40 °C*	107.3	12	**0.23**
36-40 °C	106.1	4.9	**0.6**	41-45 °C	111.2	1.8	**0.07**
41-45 °C	109.7	0.5	**0.06**	46-50 °C	114.8	0.3	**0.01**
46-50 °C	113.3	0.2	**0.03**	51-55 °C	118.4	0.1	**0.00**
> 51°C	117.7	0.1	**0.01**	> 56°C	124.8	0.0	**0.00**

Total Radiant flux (MW) = 3.0 ± 0.9

** values below 32°C and 35°C for the main crater and the southern fracture zone were considered as background since it was not possible to well descriminate the heated surface.*

Table 2. The Gamalama gas composition and ratios at three different locations.

Recording point	MG1	MG2	MG3
Gas Concentration			
H_2O (ppm v)	7000-14000	3000-12000	1000-7000
CO_2 (ppm v)	450-770	390-550	360-490
SO_2 (ppm v)	0.05-0.13	0.2-1.2	0.3-1.6
H_2S (ppm v)	0.3-0.4	0.4-6.5	0.1-2.9
H_2 (ppm v)	2.0-4.0	0.6-4.0	0.0-3.5
Gas ratios			
H_2O/SO_2	-	5895 ± 2979	3169 ± 1144
CO_2/SO_2	-	201 ± 50	76 ± 12
H_2S/SO_2	-	7.9 ± 0.9	2.5 ± 0.3
H_2/SO_2	-	1.4 ± 0.9	1.2 ± 1.0
Gas composition		Composition (mol%)	
	H_2O	97.5	
	CO_2	2.3	

SO_2	0.03
H_2S	0.08
H_2	0.04

Table 3. SO_2 flux obtained during the Jul. 2015 eruption.

19 Jul. 2015				20 Jul. 2015				21 Jul. 2015			
Scan	Start time	Flux (t/d)	Error (%)	Scan	Start time	Flux (t/d)	Error (%)	Scan	Start time	Flux (t/d)	Error (%)
1	11:22:03	2006	26	1	11:32:41	955	10	1	14:51:27	1284	29
2	11:24:01	2615	31	2	11:37:34	923	10	2	14:55:35	1180	30
3	11:25:56	2459	26	3	11:42:41	593	10	3	14:59:29	1344	30
4	11:27:52	1980	31	4	11:47:36	337	10	4	15:04:20	1062	35
5	11:29:47	2106	36	5	11:52:15	477	4	5	15:11:37	1124	29
6	11:31:41	2027	36	6	11:56:43	664	10			Mean value 1199±372 t/d	
7	11:33:36	1886	31	7	12:01:17	855	10				
8	11:35:32	1900	20	8	12:05:57	1582	6				
9	11:37:29	1669	15	9	12:10:43	1562	4				
10	11:39:25	1530	4	10	12:15:18	549	10				
11	11:41:18	1277	42	11	12:19:52	881	10				
12	11:43:15	1089	4	12	12:24:22	342	10				
13	11:45:12	872	31	13	12:28:49	1597	10				
14	11:47:09	838	26	14	12:33:19	385	10				
15	11:49:04	1098	4	15	12:37:51	617	10				
16	11:50:58	1182	1	16	12:42:33	1237	10				
17	11:52:54	1328	1	17	12:47:08	785	10				
18	11:54:50	1566	26	18	12:51:37	1123	10				
19	11:56:58	1772	4	19	12:56:39	796	10				
20	11:58:45	1889	4	20	13:01:17	1083	10				
		Mean value 1654±331 t/d		21	13:05:57	815	10				
				22	13:10:36	1147	10				
				23	13:15:33	1318	10				
				24	13:20:10	2240	10				

25	13:24:47	602	10
26	13:29:28	331	10
27	13:34:22	482	10
28	13:39:01	223	10
29	13:43:37	162	10
30	13:48:09	882	10

Mean value 851±76 t/d

Mean SO_2 flux: 1235 ± 260 t/d

Figure 1. Gamalama volcano is one of the five active volcanoes of Halmahera arc, Indonesia. The picture upper left highlights the city of Ternate situated on the southeastern flank of the volcano. The google earth satellite image shows the summit configuration.

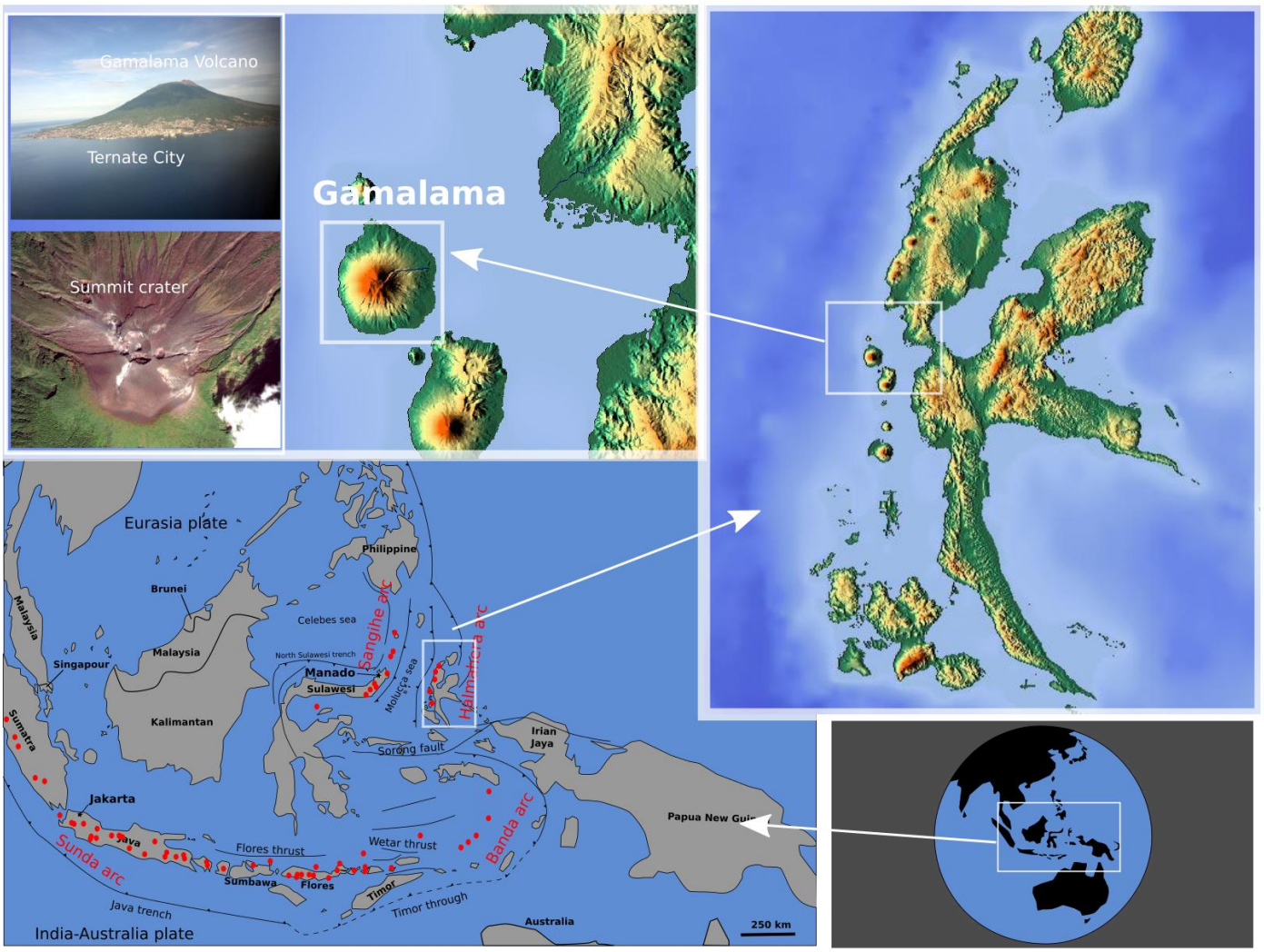

Figure 2. Heat distribution observed on Gamalama using an OPRIS PI640. The position of the IR camera is provided with the viewing direction. The above picture and the corresponding thermal mosaic provide an overview of the crater, whilst the bottom picture and the associated thermal image correspond to the southern fracture zone. The dashed line marked the hottest surface.

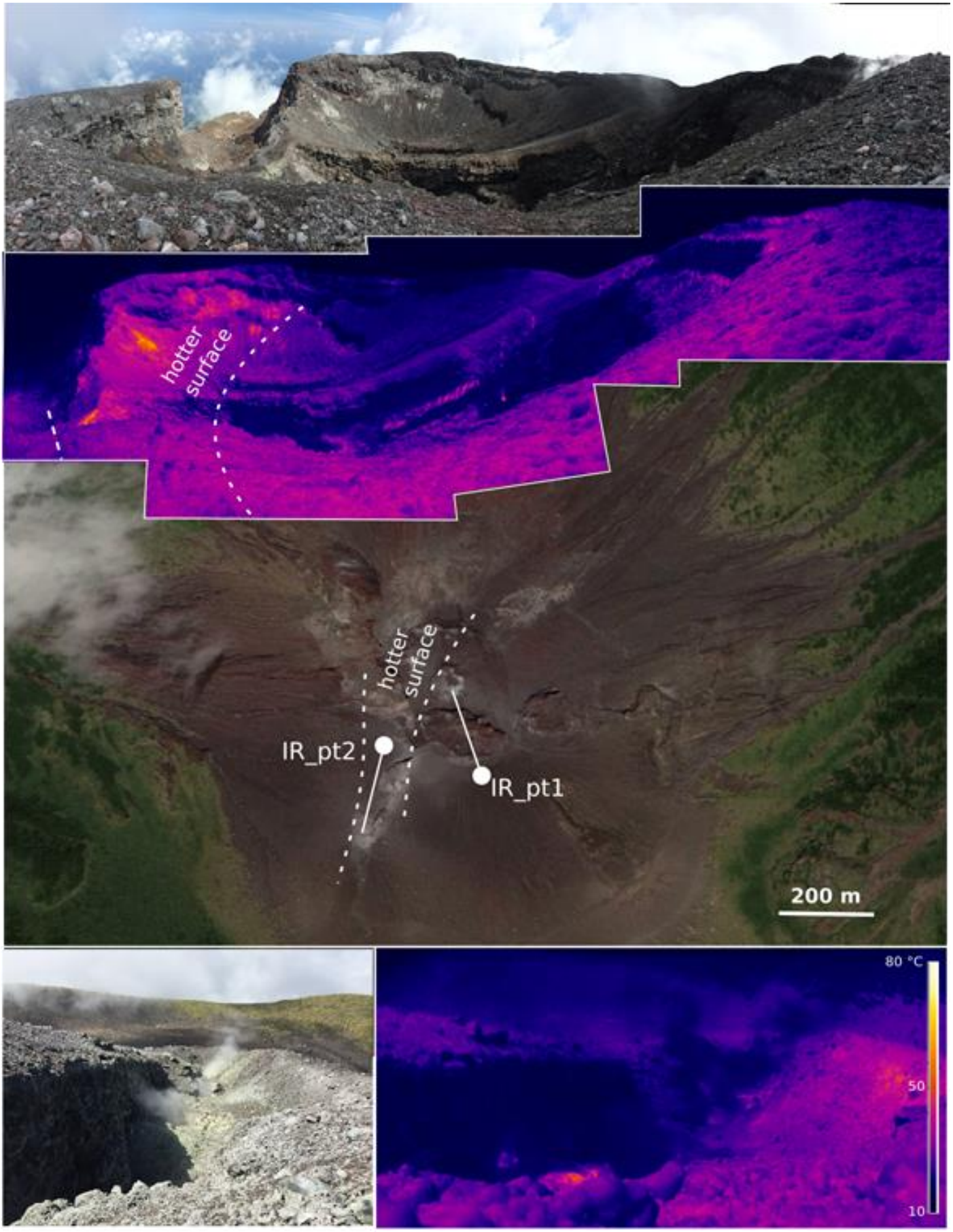
hotter surface
hotter surface
IR_pt2
IR_pt1
200 m
80 °C
50
10

Figure 3. (A) Variation of gas concentrations obtained at 3 different points (MG1, MG2, and MG3) on Gamalama summit (B). MG2 position is directly in the plume, compare to MG3, but this latter is close enough to capture the composition of single puffs. MG1 is situated outside the main active zone.

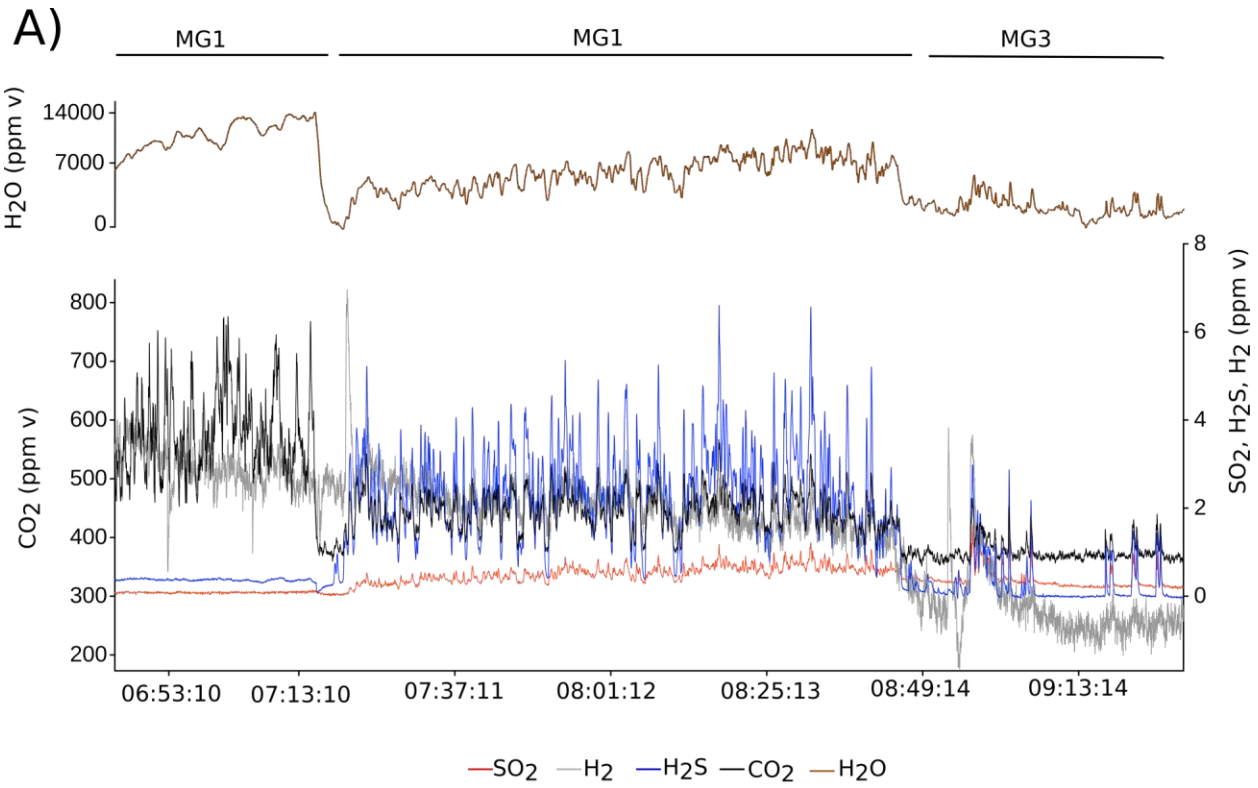
A)
MG1
MG1
MG3
H2O (ppm v)
14000
7000
0
CO2 (ppm v)
800
700
600
500
400
300
200
SO2, H2S, H2 (ppm v)
8
6
4
2
0
06:53:10
07:13:10
07:37:11
08:01:12
08:25:13
08:49:14
09:13:14
SO2
H2
H2S
CO2
H2O

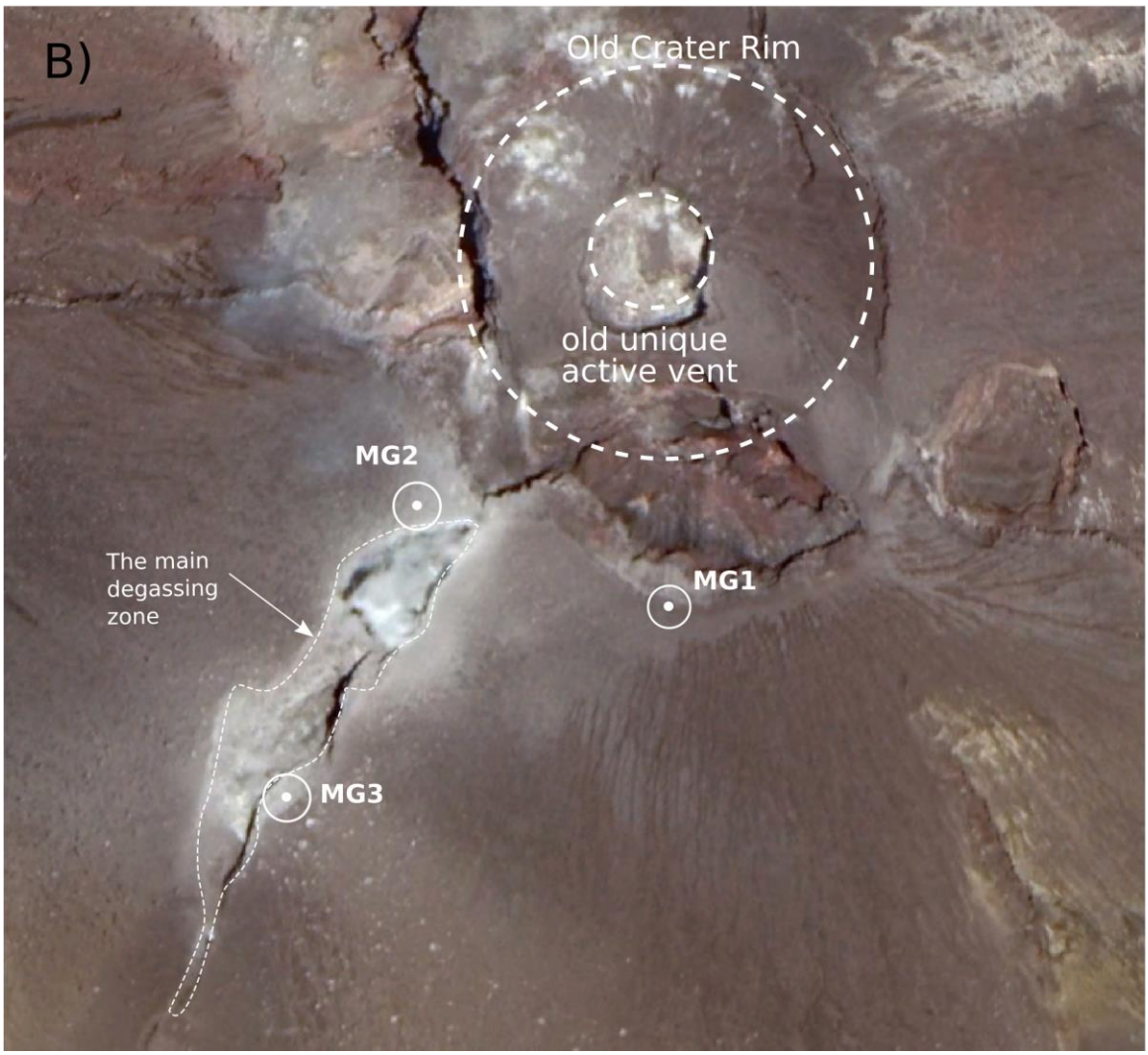
B)
Old Crater Rim
old unique
active vent
MG2
The main
degassing
zone
MG1
MG3

Figure 4. Correlation between H_2O, CO_2, H_2S, and H_2 with SO_2 for MG2 (black dots) and MG3 (red dots). H_2S vs. SO_2 shows a clear change in concentration between MG_2 and MG_3 (A). A similar change is highlighted by CO_2 (B). There is a shift towards lower H_2O concentration between MG2 and MG3 and a slight change of H_2O/SO_2 ratios (C). H_2 also shows a shift in concentration between MG2 and MG3 but the H_2/SO_2 ratios are comparable (D). Note that there is no gas correlation at MG1.

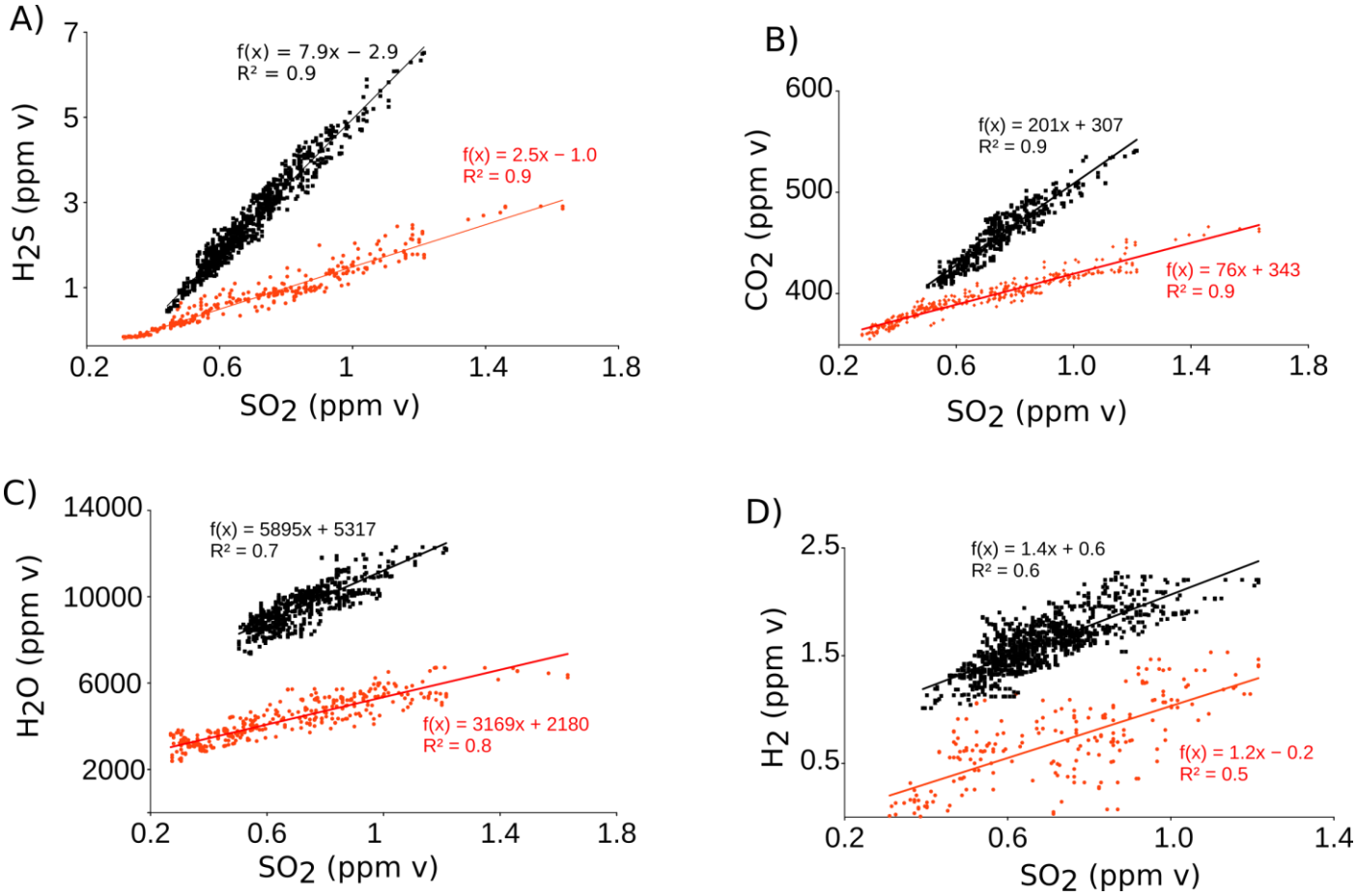

Figure 5. CO_2-H_2O-S_T discriminates the hydrothermal gas composition from Gamalama and Papandayan (Fisher and Chiodani, 2015), in comparison to the magmatic gas from other volcanoes in Indonesian, including Merapi (Fisher and Chiodani, 2015), Bromo (Aippa et al., 2015), Sirung (Bani et al., 2017), Dukono (Bani et al., 2018) and Gamkonora (Saing et al., 2020).

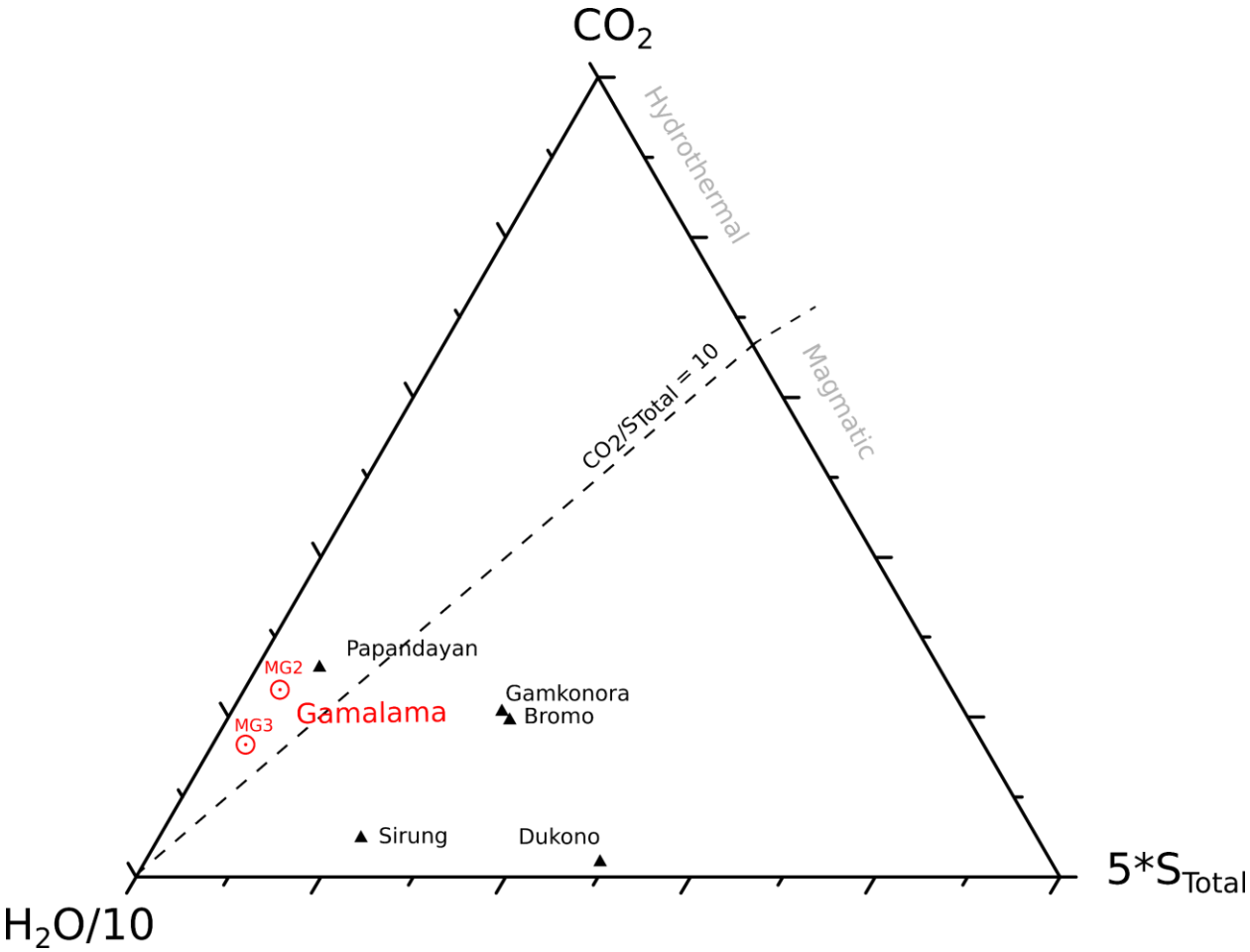

Figure 6. The CO_2/ST vs. Gas temperature (T°C) suggest contributions from hydrothermal and magmatic fluids at Gamalama, similar to Papandayan (Fisher and Chiodani, 2015).

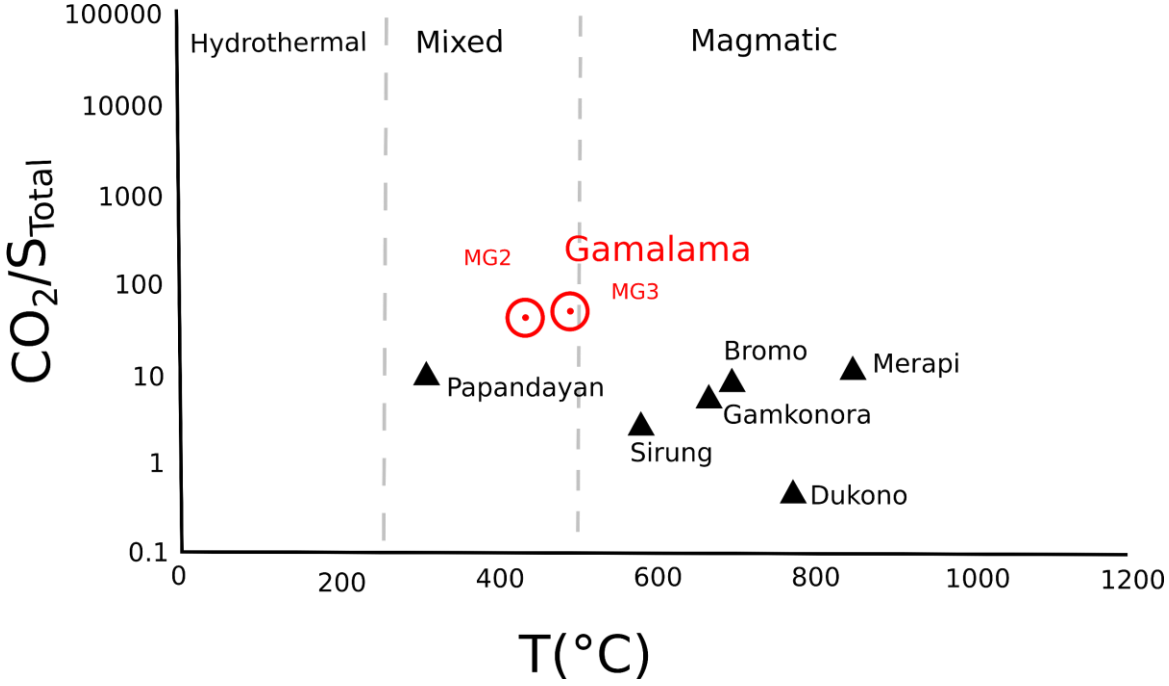

Figure 7. Fresh rock samples collected during this work at the summit of the Gamalama volcano indicate a basalt magma composition (in red - 2018). The compositions of the 1907 lava flow and the ejected

material of the 1990 eruption (Mawardi et al., 1991) are also of basaltic composition. The less differentiated melt source on Gamalama contrasts with the more differentiated sources on other volcanoes of Halmahera arc, including Gamkonora (stars), Dukono (triangles), and Ibu (squares).

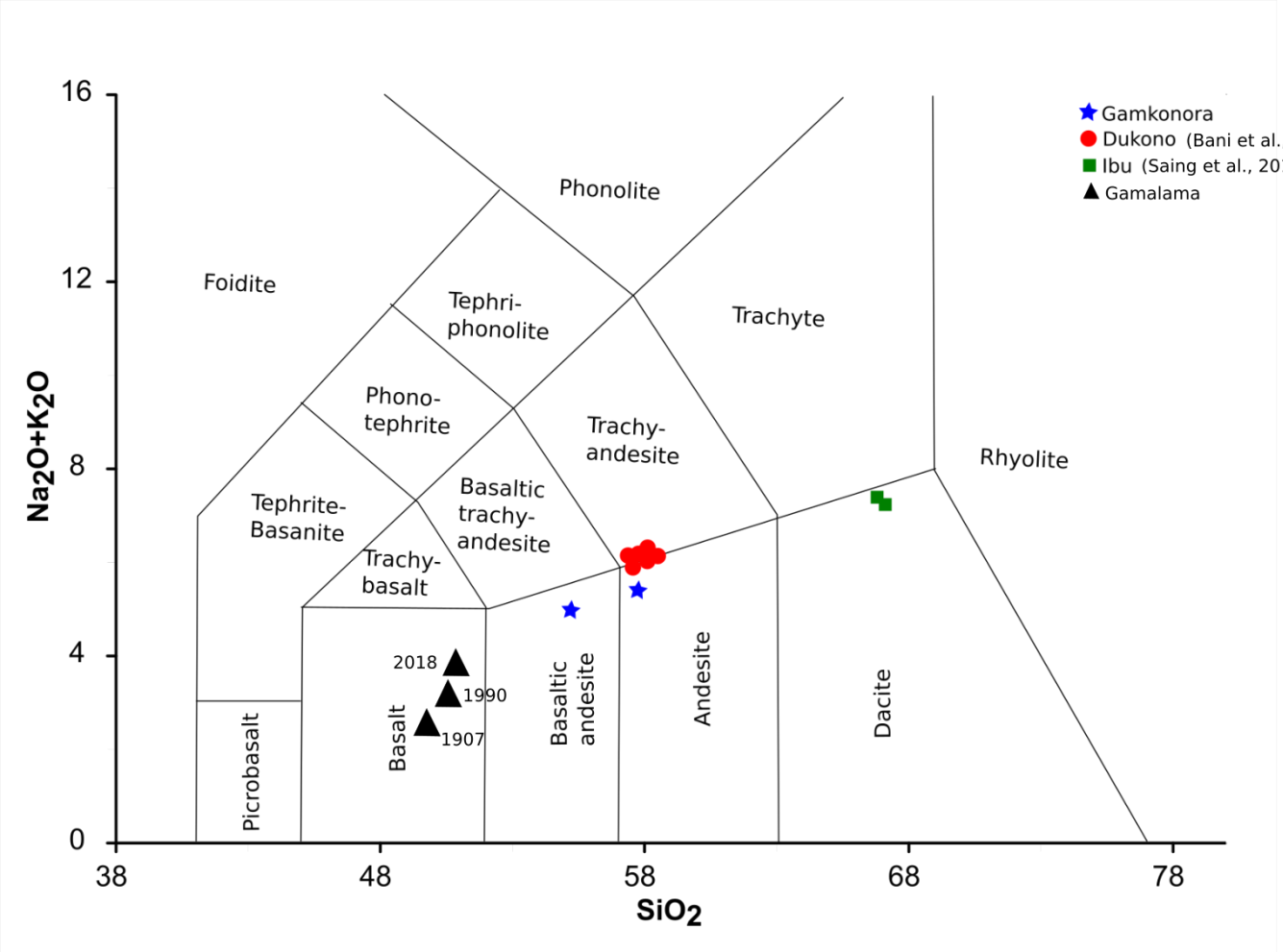

Figure 8. (A) Gamalama eruptive event of VEI 1 to 3 since 1510. The cumulative values highlight two periods of an increasing number of eruptive events. The second and most recent increase coincides with the fracture formation between 2002 and 2019. The main active zone has shifted over the same period, from the central unique active vent to the peripheral fractured active zones (B). The charts are made based on available satellite pictures in Google Earth.

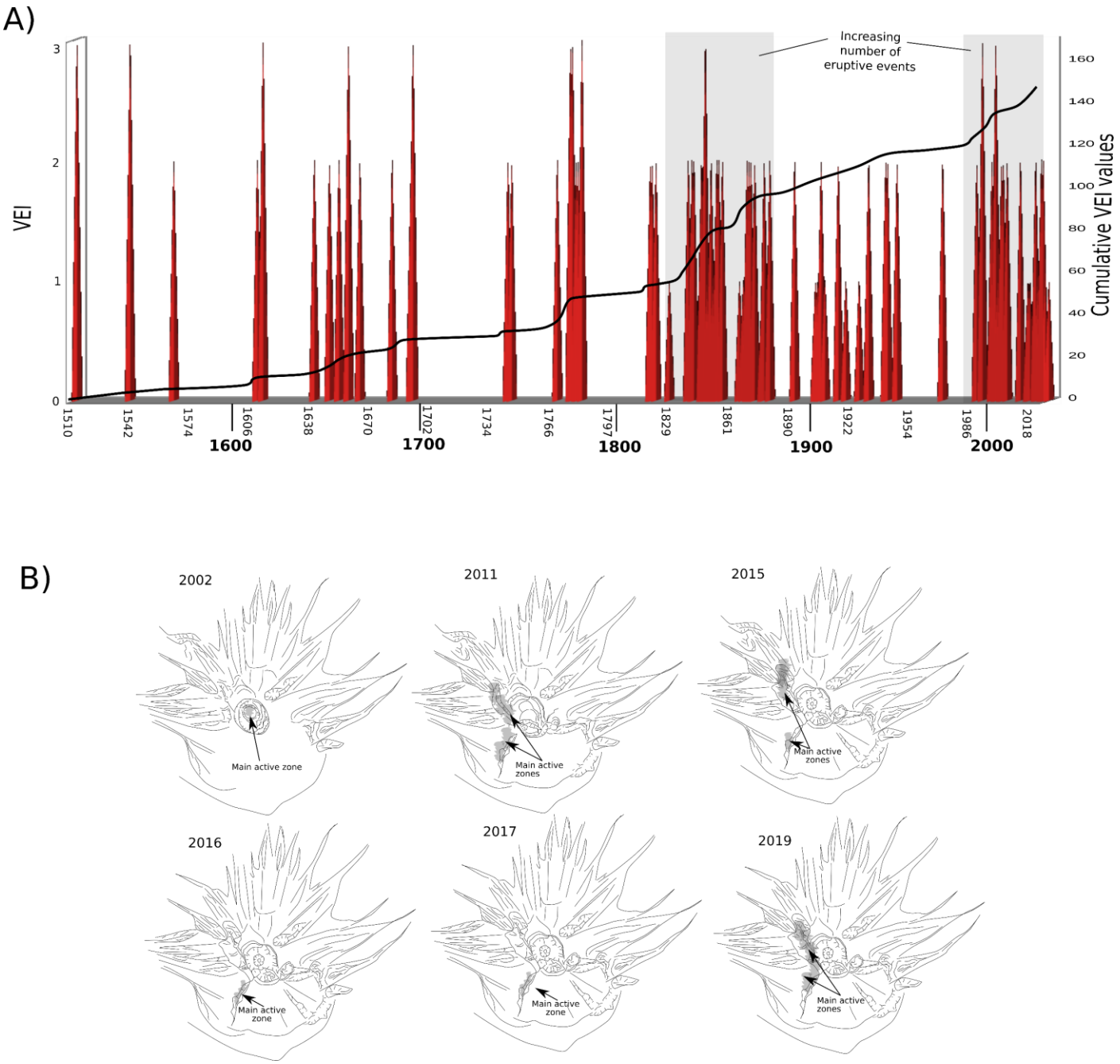

Figure 9. The magmatic fluid injected into the hydrothermal system may lead to rock alteration and sulfur precipitates, leading to the formation of a hydrothermal seal that subsequently controls the eruptive activity. The pressure developed by the hydrothermal system may exceed the tensile strength of the seal, leading to a phreatic event.

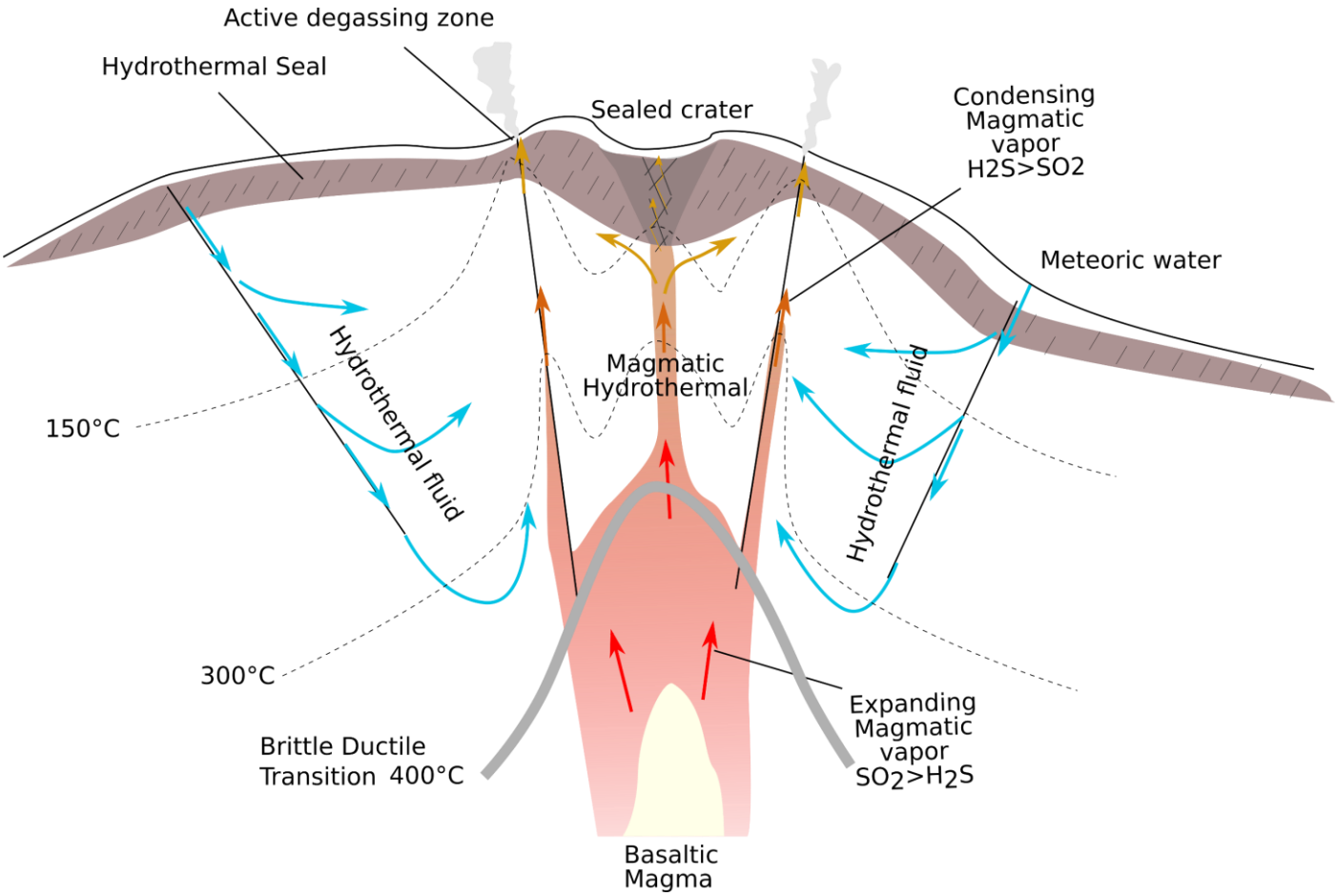
Active degassing zone
Hydrothermal Seal
Sealed crater
Condensing
Magmatic
vapor
H2S>SO2
Meteoric water
Hydrothermal fluid
Magmatic
Hydrothermal
Hydrothermal fluid
150°C
300°C
Brittle Ductile
Transition 400°C
Expanding
Magmatic
vapor
SO2>H2S
Basaltic
Magma